The lowest metallicity type II supernova from the highest mass red-supergiant progenitor

J. P. Anderson,[1*] L. Dessart,[2], C. P. Gutiérrez,[3] T. Krühler,[4] L. Galbany,[5] A. Jerkstrand,[6] S. J. Smartt,[6] C. Contreras,[7] N. Morrell,[7] M. M. Phillips,[7] M. D. Stritzinger,[8] E. Y. Hsiao,[9], S. González-Gaitán,[10,11] C. Agliozzo,[10,12] S. Castellón,[9] K. C. Chambers,[13] T. -W. Chen,[4] H. Flewelling,[13] C. Gonzalez,[7] G. Hosseinzadeh,[14,15] M. Huber,[13] M. Fraser,[16] C. Inserra,[3] E. Kankare,[6] S. Mattila,[17] E. Magnier,[13] K. Maguire,[6], T. B. Lowe,[13] J. Sollerman,[18] M. Sullivan,[3] D. R. Young,[6] S. Valenti[19]

[1]*European Southern Observatory, Alonso de Córdova 3107, Casilla 19, Santiago, Chile*

[2]*Unidad Mixta Internacional Franco-Chilena de Astronomía (CNRS UMI 3386), Departamento de Astronomía, Universidad de Chile, Camino El Observatorio 1515, Las Condes, Santiago, Chile*

[3]*School of Physics and Astronomy, University of Southampton, Southampton, SO17 1BJ, UK*

[4]*Max-Planck-Institut für extraterrestrische Physik, Giessenbachstraße, D-85748 Garching, Germany*

[5]*PITT PACC, Department of Physics and Astronomy, University of Pittsburgh, Pittsburgh, PA 15260, USA*

[6]*Astrophysics Research Centre, School of Mathematics and Physics, Queens University Belfast, Belfast BT7 1NN, UK*

[7]*Carnegie Observatories, Las Campanas Observatory, Casilla 601, La Serena, Chile*

[8]*Department of Physics and Astronomy, Aarhus University, Ny Munkegade 120, 8000 Aarhus C, Denmark*

[9]*Department of Physics, Florida State University, 77 Chieftan Way, Tallahassee, FL 32306, USA*

[10]*Millennium Institute of Astrophysics, Universidad de Chile, Casilla 36-D, Santiago, Chile*

[11]*Center for Mathematical Modelling, University of Chile, Beauchef 851, Santiago, Chile*

[12]*Departamento de Ciencias Fisicas, Universidad Andres Bello, Avda. Republica 252, Santiago, Chile*

[13]*Institute for Astronomy, University of Hawaii, 2680 Woodlawn Drive, Honolulu, HI 96822*

[14]*Las Cumbres Observatory, 6740 Cortona Dr Ste 102, Goleta, CA 93117-5575, USA*

[15]*Department of Physics, University of California, Santa Barbara, CA 93106-9530, USA*

[16]*O'Brien Centre for Science, North University College Dublin, Belfield, Dublin 4, Ireland*

[17]*Tuorla Observatory, Department of Physics and Astronomy, University of Turku, Väisäläntie 20, 21500, Piikkiö, Finland*

[18]*Department of Astronomy and the Oskar Klein Centre, Stockholm University, AlbaNova, SE-106 91 Stockholm, Sweden*

[19]*Department of Physics, University of California, Davis, CA 95616, USA*

Red supergiants have been confirmed as the progenitor stars of the majority of hydrogen-rich type II supernovae[1]. However, while such stars are observed with masses $>$25 $\mathrm{M}_{\odot}$[2], detections of $>$18 $\mathrm{M}_{\odot}$ progenitors remain elusive[1]. Red supergiants are also expected to form at all metallicities, but discoveries of explosions from low-metallicity progenitors are scarce. Here, we report observations of the type II supernova, SN 2015bs, for which we infer a progenitor metallicity of $\leq$0.1 $\mathrm{Z}_{\odot}$ from comparison to photospheric-phase spectral models[3], and a Zero Age Main-Sequence mass of 17-25 $\mathrm{M}_{\odot}$ through comparison to nebular-phase spectral models[4,5]. SN 2015bs displays a normal 'plateau' light-curve morphology, and typical spec-

tral properties, implying a red supergiant progenitor. This is the first example of such a high mass progenitor for a 'normal' type II supernova, suggesting a link between high mass red supergiant explosions and low-metallicity progenitors.

Type II supernovae (SNe II) are the most abundant stellar explosions in the Universe, as measured in volume-limited samples[6]. (We use 'SNe II' to refer to all objects showing flat or declining V-band light curves, together with broad Hα features, excluding type IIn, IIb and SN 1987A-like events.) They are the only SN type with robust constraints on their progenitor stars[1], providing direct evidence for red supergiant (RSG) progenitors and confirming results from light-curve modelling[7]. Pre-explosion images constrain their initial mass to be 8.5-18 $\mathrm{M}_{\odot}$[1]. The lack of progenitors above this mass is referred to as the 'red supergiant problem'[8], given that at least some stars $>$18 $\mathrm{M}_{\odot}$ should be viable SN II progenitors[9], with the exact mass limit being dependent on rotation, metallicity and mass-loss[10,11]. This is also seen when comparing nebular-phase spectra ($>$200 days post explosion, +200 d) with SN II explosion models[4,5,12–14]. A number of solutions to this issue have been proposed. [15] suggested that the inclusion of unaccounted for circumstellar dust around progenitors could translate to higher luminosities and therefore higher masses. It has been argued that the problem disappears if accurate bolometric corrections are used to estimate progenitor luminosities[16]. The predicted upper mass limit for producing SNe II decreases in rotating models[10] and when employing higher RSG mass-loss rates[11]. This opens the possibility that progenitors above 20 $\mathrm{M}_{\odot}$ may not explode as SNe II, but as SNe IIb or SNe Ib. However, it has also been argued[1] that this dearth of massive progenitors is due to RSGs collapsing to a black holes with no (or a weak/faint) accompanying SN. This latter scenario is supported by the observed bimodal distribution of compact remnants[17], and the recent detection of a vanishing 25 $M_\odot$ RSG star[18].

Historical SN surveys prioritised SN detection over completeness concentrating on observations of bright, nearby galaxies, where the majority of the star formation (SF) takes place at solar metallicity. This led to a lack of SNe found in low-luminosity, low-metallicity galaxies. While modern surveys are rectifying this situation[19], samples of SNe II in hosts of low metallicity ($\leq$0.5 $Z_\odot$) are still lacking[20–22]. We therefore started a follow-up program to study SNe II discovered in galaxies dimmer than –18.5 in the B-band, through the *Public ESO Spectroscopic Survey of Transient Objects* (PESSTO)[23].

On the 25th of September 2014, the *Catalina Real-Time Transient Survey* (CRTS)[24] discovered the apparently host-less SN CSS140925:223344-062208. It was also recovered by the CRTS in the Mount Lemmon facility, and detected by the *Panoramic Survey Telescope and Rapid Response System* (Pan-STARRS1[25]: https://star.pst.qub.ac.uk/ps1threepi/psdb/, hereafter the SN is designated as the IAU confirmed name of SN 2015bs). A pre-SN non detection constrains its explosion epoch to be the 20th of September ±5 days. The classification spectrum revealed Balmer lines on top of a blue continuum, indicative of a young SN II. A redshift of around 0.02 was estimated from the SN spectrum. Three additional optical spectra were obtained during the plateau phase, together with B, V, r, i photometry. A year post explosion we also obtained integral field spectroscopy of SN 2015bs and its surroundings.

SN 2015bs displays a relatively luminous, but normal optical light-curve (Fig. 1, and Supplementary Information, SI). At $\sim$50 d, the spectrum of SN 2015bs is dominated by the typical hydrogen Balmer lines observed in SNe II (Fig. 2a). However, metal absorption lines are much less prominent in comparison to other SNe II. Spectral models produced from progenitors of different metallicity[3,21] show that as metallicity decreases metal-line pseudo-equivalent widths become weaker. Further, SNe II occurring within lower-metallicity H II regions display weaker Fe II 5018 Å lines[22]. Fig. 3 shows how the +57 d spectrum of SN 2015bs is well matched by a mode at 0.1 $Z_\odot$, in contrast with SN 2012aw, whose strong metal lines support a super-solar metallicity progenitor. Measuring the pseudo equivalent width of the Fe II 5018 Å line, we find 4.25±0.54 Å for SN 2015bs, and 3.61±1.29 Å for the 0.1 $Z_\odot$ model (11.33±0.71 Å is measured for the 0.4 $Z_\odot$ model), in support of a low-metallicity progenitor.

Using our late-time spectroscopy, we identify the host of SN 2015bs at an angular separation of 3.4″ from the SN (see SI Fig. 1) that shows narrow Hα (from ionised gas within the galaxy) at a redshift of 0.027, consistent with the spectra of SN 2015bs. We measure an absolute r-band magnitude for the host of –12.2 mag. This makes SN 2015bs the lowest-luminosity host for a SN II, being more than a magnitude fainter than the previously dimmest host[19,20,26]. Using well known galaxy luminosity–metallicity relationships this translates to a host metallicity of 0.04 $Z_\odot$±0.05[19,27].

In addition to being the lowest metallicity SN II studied to-date (as compared to all previous published SN II environment metallicities[20,26]), SN 2015bs is unique in its nebular phase. It presents striking differences compared to other SNe II (Fig. 2b). Dominant spectral lines at these epochs are [O I] 6300,6364 Å, Hα, and [Ca II] 7291,7323 Å. In SN 2015bs [O I] is as strong as Hα and [Ca II]: in most other SNe II Hα is stronger than either line, and [Ca II] is stronger than [O I]. In addition, the nebular hydrogen line of SN 2015bs (Supplementary Fig. 8) is broader than seen in other SNe II. Observations at nebular epochs can be used to constrain the properties of the helium core. Following the the tight relation between helium-core mass and ZAMS[28] (that is largely insensitive to metallicity$\sim$30 $\mathrm{M}_{\odot}$[3,9]), we thus constrain the progenitor mass of SN 2015bs. One caveat is the way convection is treated in 1-D models, and the associated uncertainties[29] that may complicate the exact mapping to ZAMS mass.

The absolute strength of [O I] is an indicator of the helium core mass, and nebular modelling of SNe II reveals that as progenitor mass increases so does the strength of [O I] as compared to Hα and [Ca II][5,30]. Our observations therefore suggest that SN 2015bs was the explosion of a higher mass progenitor than previously observed SN II. In the Supplementary Information (SI) we make comparisons between the +413 d spectrum of SN 2015bs and spectra from 15 and 25 $\mathrm{M}_{\odot}$ ZAMS models[12] (Supplementary Fig. 11). SN 2015bs displays significantly stronger [O I] than the 15 $\mathrm{M}_{\odot}$ model, suggesting a higher mass progenitor than previous nebular-spectroscopic constraints.

We make quantitative comparisons between SN 2015bs, our comparison SN II sample, and models, using the percentage of the [O I] flux with respect to the total optical flux contained within the wavelength range of the nebular SN 2015bs spectrum (see Table 1). This is an alternative to using the luminosity of [O I] normalised to the ^{56}Co decay power. The ^{56}Co-normalisation method has been used[5] because gamma-ray trapping also depends on ZAMS mass, errors from extinction are moderated as the luminosity of [O I] and the ^{56}Ni mass estimates are affected similarly, and contamination by background continuum is removed. Using the optical ratio removes uncertainties associated to bolometric corrections used to estimate ^{56}Ni masses. SN 2015bs has a value of 15.4±0.7%, which is at least twice higher than previously observed. This provides further evidence that SN 2015bs arose from the highest mass SN II progenitor to date. SN 2015bs is closer to the percentage of the 19 $\mathrm{M}_{\odot}$ model than that of 15 $\mathrm{M}_{\odot}$ (Table 1), and we here constrain its progenitor mass to be 17-18 $\mathrm{M}_{\odot}$. Such a mass constraint lies at the upper limit of the mass range from direct progenitor detections – while being larger than any previous nebular-spectrum constraints. However, it is clear from Fig. 2b that the nebular spectrum of SN 2015bs is significantly distinct from other SNe II. There is therefore a real difference in helium-core mass (and therefore progenitor mass) between SN 2015bs and previously studied RSG explosions.

One should note that model line fluxes start to saturate above 19 $\mathrm{M}_{\odot}$ due to line absorption in the increasingly dense cores (see the relatively small increase in the [O I] percentage for the 25 $\mathrm{M}_{\odot}$ model). This means that models in the 20-30 $\mathrm{M}_{\odot}$ range are only 20-30% brighter in [O I] than measured values, and cannot be ruled out considering model uncertainties. At the same time, model tracks at 20-25 $\mathrm{M}_{\odot}$ are still over a factor of 3-6 brighter than 12-15 $\mathrm{M}_{\odot}$ models, outlining the diagnostic power of using [O I] to determine progenitor mass. No previous SN II nebular spectrum was consistent with models of ZAMS of much more than 15 $\mathrm{M}_{\odot}$, whereas – within measurement and model uncertainties – SN 2015bs is consistent with models of 19 $\mathrm{M}_{\odot}$ and above.

The broad nebular Hα emission of SN 2015bs can also be explained through the explosion of a star with a higher helium-core mass. In SNe II, the width of the nebular lines reflect the velocity of the outer edge of the helium core, or equivalently the inner edge of the hydrogen-rich envelope[4]. Since the width of optical lines in SN 2015bs during the photospheric phase suggests a standard explosion energy, this implies a larger fractional core mass, i.e. the helium-core material represents a larger fraction of the total mass and its outer edge is closer to the maximum velocity in the ejecta[4]. The high Hα nebular velocity of SN 2015bs (seen in Supplementary Figs 7 and 8), therefore provides further evidence that SN 2015bs had a massive helium core. SN 2015bs has a Half-Width at Half Maximum (HWHM) nebular Hα velocity of $2127 \pm 308\,\mathrm{kms}^{-1}$, while inferred photospheric velocity at +50 d is $5359 \pm 392\,\mathrm{kms}^{-1}$. Making direct comparison to the hydrodynamic models of [4] (specifically velocities in their table 2), constrains the progenitor mass of SN 2015bs to be between 20 and 25 $\mathrm{M}_{\odot}$. While the velocity of the Hα nebular line is significantly higher for SN 2015bs than for any other SN II, the velocities of [O I] are similar between SN 2015bs and the comparison sample (see Supplementary Fig. 7). In low-mass SNe II (ZAMS $\leq$12 $\mathrm{M}_{\odot}$), as much as $\sim$50% of the nebular line emission of [O I] and the majority of [Ca II] arises from the hydrogen-rich envelope, with the rest coming from the core[5,31]. However, assuming a higher mass for SN 2015bs, [O I] emission becomes dominated by oxygen in the core rather than primordial oxygen in the envelope. This naturally explains the relatively high ratio of hydrogen to oxygen velocities as compared to other SNe II (dominated by lower core-mass events), and gives further support for a 20-25 $\mathrm{M}_{\odot}$ progenitor for SN 2015bs. We note that such a difference between Hα and [O I] line velocities was also observed in SN 1987A[31], whose progenitor was also of relatively low metallicity and high mass.

The association of SN 2015bs with a 17-25 $\mathrm{M}_{\odot}$ progenitor star at 0.1 $\mathrm{Z}_{\odot}$ has important implication for massive star evolution and explosions. Firstly, it shows that stars more massive than 17 $\mathrm{M}_{\odot}$ can explode, and that not all such massive progenitors proceed to direct black-hole formation without any accompanying bright transient. Together with the recent identification of a vanishing 25 $\mathrm{M}_{\odot}$ RSG star[18], this supports the notion that there may be 'islands of explodability' for massive stars[32]: the generally greater mass accretion rate onto the proto-neutron star forming in higher mass stars may not systematically lead to a failed explosion[33]. Secondly, the link between a high-mass RSG explosion and a low-metallicity progenitor opens the possibility that progenitors $>20\ \mathrm{M}_{\odot}$ can successfully explode as SNe II *if* the metallicity is sufficiently low (mass-loss is lower), while at solar metallicities the majority of such RSGs may lose enough mass to explode as SNe IIb or Ib (although the detection of a disappearing high-mass RSG at solar metallicity provides an obvious counter example that this is not always the case). A detection of a high-mass and metallicity progenitor for such SNe would provide confirmation of this possibility. These different interpretations are discussed further in the SI.

We have presented observations of SN 2015bs, a type II SN that exploded in the lowest-luminosity host galaxy for any SN II discovered to date[19,20,26]. The weakness of metal lines in the photospheric-phase spectrum is consistent with models of SNe II at low metallicity, and confirms the utility of SNe II as metallicity indicators[21,22]. The nebular spectrum is notably distinct, implying a more massive progenitor than all previously known SNe II. The effects of sub-Small Magellanic Cloud metallicities ($<0.4\ \mathrm{Z}_{\odot}$) on SNe II and massive star evolution are relatively unconstrained observationally. The unique characteristics of SN 2015bs highlights the bias in the current sample of SNe II, with most events studied at around solar metallicity. Current and future surveys will broaden the SN II parameter space, and further our knowledge of the evolution and explosion of massive stars.

References

1. Smartt, S. J. Observational Constraints on the Progenitors of Core-Collapse Supernovae: The Case for Missing High-Mass Stars. *Pub. Astro. Soc. Aust.* **32**, 16-38 (2015)

2. Levesque, E. M. *et al.* The Effective Temperature Scale of Galactic Red Supergiants: Cool, but Not As Cool As We Thought. *Astrophys. J.* **628**, 973-985 (2005).

3. Dessart, L. *et al.* Type II-Plateau supernova radiation: dependences on progenitor and explosion properties. *Mon. Not. R. Astron. Soc.* **433**, 1745-1763 (2013)

4. Dessart, L. *et al.* Determining the main-sequence mass of Type II supernova progenitors. *Mon. Not. R. Astron. Soc.* **408**, 827-840 (2010)

5. Jerkstrand, A. *et al.* The progenitor mass of the Type IIP supernova SN 2004et from late-time spectral modeling *Astron. Astrophys*. **546**, 28-49 (2012)

6. Li, W. *et al.* Nearby supernova rates from the Lick Observatory Supernova Search - II. The observed luminosity functions and fractions of supernovae in a complete sample. *Mon. Not. R. Astron. Soc.* **412**, 1441-1472 (2011)

7. Falk, S. W. & Arnett, W. D. Radiation Dynamics, Envelope Ejection, and Supernova Light Curves. *Astrom. Astrophys. Suppl. S*. **33**, 515-562 (1977)

8. Smartt, S. J., *et al.* The death of massive stars - I. Observational constraints on the progenitors of Type II-P supernovae. *Mon. Not. R. Astron. Soc.* **395**, 1409-1437 (2009)

9. Woosley, S. E. *et al.* The evolution and explosion of massive stars. *Rev. Mod. Phys.*. **74**, 1015-1071 (2002)

10. Hirschi, R., Meynet, G. & Maeder, A. Stellar evolution with rotation. XII. Pre-supernova models. *Astron. Astrophys.* **425**, 649-670 (2004)

11. Chieffi, A. & Limongi, M. Pre-supernova Evolution of Rotating Solar Metallicity Stars in the Mass Range 13-120 $\mathrm{M}_{\odot}$ and their Explosive Yields. *Astrophys. J.* **764**, 21-57 (2013)

12. Jerkstrand, A. *et al.* The nebular spectra of SN 2012aw and constraints on stellar nucleosynthesis from oxygen emission lines. *Mon. Not. R. Astron. Soc.* **439**, 3694-3703 (2014)

13. Jerkstrand, A. *et al.* Supersolar Ni/Fe production in the Type IIP SN 2012ec *Mon. Not. R. Astron. Soc.* **448**, 2482-2494 (2015)

14. Silverman, J. M. *et al.* After the Fall: Late-Time Spectroscopy of Type IIP Supernovae. *Mon. Not. R. Astron. Soc.* **467**, 369-411 (2017)

15. Walmswell, J. J. & Eldridge, J. J. Circumstellar dust as a solution to the red supergiant supernova progenitor problem. *Mon. Not. R. Astron. Soc.* **419**, 2054-2062 (2012)

16. Davies, B. & Beasor, E. R. The initial masses of the red supergiant progenitors to Type II supernovae. *Mon. Not. R. Astron. Soc.* **474**, 2116-2128 (2018)

17. Kochanek, C. S. Failed Supernovae Explain the Compact Remnant Mass Function. *Astrophys. J.* **785**, 28-34 (2014)

18. Adams, S. M. *et al.* The search for failed supernovae with the Large Binocular Telescope: confirmation of a disappearing star. *Mon. Not. R. Astron. Soc.* **468**, 4968-4981 (2017)

19. Arcavi, I. *et al.* Core-collapse Supernovae from the Palomar Transient Factory: Indications for a Different Population in Dwarf Galaxies. *Astrophys. J.* **721**, 777-784 (2010)

20. Stoll, R. *et al.* Probing the Low-redshift Star Formation Rate as a Function of Metallicity through the Local Environments of Type II Supernovae. *Mon. Not. R. Astron. Soc.* **773**, 12-31 (2013)

21. Dessart, L. *et al.* Type II Plateau supernovae as metallicity probes of the Universe. *Mon. Not. R. Astron. Soc.* **440**, 1856-1864 (2014)

22. Anderson, J. P. *et al.* Type II supernovae as probes of environment metallicity: observations of host H II regions. *Astron. Astrophys*. **589**, 110-130 (2016)

23. Smartt, S. J. *et al.* PESSTO: survey description and products from the first data release by the Public ESO Spectroscopic Survey of Transient Objects. *Astron. Astrophys*. **579**, 40-65 (2015)

24. Drake, A. J. *et al.* First Results from the Catalina Real-Time Transient Survey. *Astrophys. J.* **696**, 870-884 (2009)

25. Huber, M. *et al.* The Pan-STARRS Survey for Transients (PSST) - first announcement and public release. *ATEL*. **7153**, 1 (2015)

26. Taddia, F. *et al.* Metallicity from Type II supernovae from the (i)PTF. *Astron. Astrophys*. **587**, 7-13 (2016)

27. Tremonti, C. A. *et al.* The Origin of the Mass-Metallicity Relation: Insights from 53,000 Star-forming Galaxies in the Sloan Digital Sky Survey. *Astrophys. J.* **613**, 898-913 (2004)

28. Woosley, S. E. & Weaver, T. A. The Evolution and Explosion of Massive Stars. II. Explosive Hydrodynamics and Nucleosynthesis. *Astrophys. J. Suppl. S.* **101**, 181 (1995)

29. Arnett, W. D. & Meakin, C. Toward Realistic Progenitors of Core-collapse Supernovae. *Astrophys. J.* **733**, 78 (2011)

30. Fransson, C. & Chevalier, R. A. Late emission from SN 1987A. *Astrophys. J.* **322**, L15-L20 (1987)

31. Maguire, K. *et al.* Constraining the physical properties of Type II-Plateau supernovae using nebular phase spectra. *Mon. Not. R. Astron. Soc.* **420**, 3451-3468 (2012)

32. O'Connor, E. & Ott, C. D. Black Hole Formation in Failing Core-Collapse Supernovae. *Astrophys. J.* **730**, 70-90 (2011)

33. Mueller, B. *et al.* New Two-dimensional Models of Supernova Explosions by the Neutrino-heating Mechanism: Evidence for Different Instability Regimes in Collapsing Stellar Cores. *Astrophys. J.* **761**, 72-84 (2012)

Acknowledgements TK and TWC acknowledges support through the Sofja Kovalevskaja Award to P. Schady from the Alexander von Humboldt Foundation of Germany. AJ acknowledges funding by the European Unions Framework Programme for Research and Innovation Horizon 2020 under Marie Sklodowska-Curie grant agreement No 702538. SJS acknowledges funding from the European Research Council under the European Union's Seventh Framework Programme (FP7/2007-2013)/ERC Grant agreement no [291222] and STFC grants ST/I001123/1 and ST/L000709/1. MDS, CC and EH gratefully acknowledge the generous support provided by the Danish Agency for Science and Technology and Innovation realized through a Sapere Aude Level 2 grant. MDS acknowledges funding by a research grant (13261) from the VILLUM FONDEN. Support for SG is provided by the Ministry of Economy, Development, and Tourism's Millennium Science Initiative through grant IC120009 awarded to The Millennium Institute of Astrophysics (MAS), and CONICYT through FONDECYT grant 3140566. Support for CA is provided by the Ministry of Economy, Development, and Tourism's Millennium Science Initiative through grant IC120009 awarded to The Millennium Institute of Astrophysics (MAS), and CONICYT through FONDECYT grant 3150463. MF acknowledges the support of a Royal Society - Science Foundation Ireland University Research Fellowship. KM acknowledges support from the STFC through an Ernest Rutherford Fellowship. MS acknowledges support from EU/FP7-ERC grant 615929. The work of the CSP-II has been supported by the National Science Foundation under grants AST0306969, AST0607438, AST1008343, and AST1613426. This work is based (in part) on observations collected at the European Organisation for Astronomical Research in the Southern Hemisphere, Chile as part of PESSTO, (the Public ESO Spectroscopic Survey for Transient Objects) ESO program 188.D-3003, 191.D-0935. This work is based (in part) on observations collected at the European Organisation for Astronomical Research in the Southern Hemisphere under ESO programme 296.D-5003(A). This work was partly supported by the European Union FP7 programme through ERC grant number 320360. Pan-STARRS is supported by NASA grants NNX08AR22G, NNX14AM74G. PS1 surveys acknowledge the PS1SC: University of Hawaii, MPIA Heidelberg, MPE Garching, Johns Hopkins University, Durham University, University of Edinburgh, Queens University Belfast, Harvard-Smithsonian CfA, LCOGT, NCU Taiwan, STScI, University of Maryland, Eotvos Lorand University, Los Alamos National Laboratory, and NSF grant No. AST-1238877. Avishay Gal-Yam, Melina Bersten, Francisco Förster, John Hillier, Francesco Taddia and Claus Fransson are thanked for useful discussions. This research has made use of: the NASA/IPAC Extragalactic Database (NED) which is operated by the Jet Propulsion Laboratory, California Institute of Technology, under contract with the National Aeronautics; IRAF, which is distributed by the National Optical Astronomy Observatory, which is operated by the Association of Universities for Research in Astronomy (AURA) under cooperative agreement with the National Science Foundation; QfitsView; and the SDSS, funding for the SDSS and SDSS-II has been provided by the Alfred P. Sloan Foundation, the Participating Institutions, the National Science Foundation, the U.S. Department of Energy, the National Aeronautics and Space Administration, the Japanese Monbukagakusho, the Max Planck Society, and the Higher Education Funding Council for England. The SDSS Web Site is http://www.sdss.org/.

Author contributions JPA performed the analysis and wrote the manuscript. LD helped write the manuscript and provided comments on the physical interpretation. CPG provided specific measurements of pEWs of spectral lines and was part of the overall project to obtain these data. TK reduced the MUSE dataset. LG helped obtain the MUSE dataset. AJ provided comments on the physical interpretation of the nebular spectral comparisons. SJS is PI of the PESSTO project, through which spectra were obtained. CC provided calibrated photometry from the CSP-II. NM obtained the photometry from the CSP-II. MMP is PI of the CSP, which provided photometric data. MS is co-I on the CSP, which provided photometric data. EYH is co-I on the CSP, which provided photometric data. SGG analysed the light-curve data of SN 2015bs. CA was part of the PESSTO project, through which spectra were obtained. SC obtained the photometry from the CSP-II. KCC provided photometry through the Pan-STARRS project. TWC was part of the PESSTO project, through which spectra were obtained. CG obtained the photometry from the CSP-II. GH provided a spectrum from LCO. MH provided photometry through the Pan-STARRS project. MF was part of the PESSTO project, through which spectra were obtained. CI was part of the PESSTO project, through which spectra were obtained. EK was part of the PESSTO project, through which spectra were obtained. SM was part of the PESSTO project, through which spectra were obtained. EM provided photometry through the Pan-STARRS project. KM was part of the PESSTO project, through which spectra were obtained. TBL provided photometry through the Pan-STARRS project. JS was part of the PESSTO project, through which spectra were obtained. MS was part of the PESSTO project, through which spectra were obtained. DY was part of the PESSTO project, through which spectra were obtained. SV was part of the PESSTO project, through which spectra were obtained.

Competing Interests The authors declare that they have no competing financial interests.

Correspondence Correspondence and requests for materials should be addressed to J. P. Anderson (email: janderso@eso.org).

Figure 1: Comparison of optical-wavelength spectra of SN 2015bs with literature SNe II. *a):* photospheric phase spectra. While the Balmer lines appear similar between SN 2015bs and the comparison SNe, there is a clear lack of spectral features in the blue part of the spectrum. The position of the Fe II 5018 Å absorption line is indicated, bracketed by dotted black vertical lines. This line has been used as a proxy for progenitor metallicity[22], and is significantly weaker in SN 2015bs. *b):* nebular phase spectra. The most prominent nebular lines are indicated on the spectrum of SN 2013ej: [O I] 6300,6364 Å; Hα; and [Ca II] 7291,7323 Å. While the comparison SNe II all look quite similar – apart from small changes in the width of emission lines – SN 2015bs is clearly distinct. The relative strength of oxygen is much higher, and in particular Hα is broader.

SN	Epoch (days post explosion)	[O I] percentage (error)
2015bs	413	15.4 (0.7)
1999em	391	5.2 (1.0)
2004et	401	5.7 (0.9)
2007aa	376	6.1 (0.7)
2009N	406	3.0 (1.0)
2012A	393	6.6 (0.4)
2012aw	451	8.0 (0.9)
2013ej	388	8.7 (0.8)
12 $M_{\odot}$	400	4.1 (0.4)
15 $M_{\odot}$	400	8.6 (0.6)
19 $M_{\odot}$	400	17.9 (0.8)
25 $M_{\odot}$	400	19.6 (1.0)
1987A	398	9.1 (0.3)

Table 1: Measured [O I] 6300,6364 Å fluxes for SN 2015bs and our comparison SN II sample as a percentage of total 'optical' flux (4800 to 9300 Å). In the first column we list the SN name, followed by the epoch of the nebular spectrum (days post explosion) in column 2. In column 3 we present the [O I] 6300,6364 Å flux as a percentage of the total 'optical' flux. Note, for the 19 $M_{\odot}$ model this value is calculated by interpolating between nebular model spectra at +369 and +451 d. We also include values for SN 1987A for comparison. Errors on percentages are derived from the standard deviation of multiple flux measurements while making slight changes to the defined continuum level. While our model comparison suggests a ZAMS mass between 17-18 $M_{\odot}$, the [O I] percentage for the 25 $M_{\odot}$ model is not significantly higher than the 19 $M_{\odot}$ model. In addition, SN 2015bs shows a much larger value than SN 1987A, for which a 18-20 $M_{\odot}$ progenitor has been invoked.

Methods

1. CSS140925:223344-062208, aka SN 2015bs

SN 2015bs was discovered on the 25th of September 2014 by the *Catalina Sky Survey* (CSS) telescope of the overall CRTS project. In Supplementary Fig. 1 the position of the SN is indicated on a collapsed image produced from our integral field spectroscopy obtained using the *Multi Unit Spectroscopic Explorer* (MUSE[34]) at the *Very Large Telescope*, VLT. While no explosion-epoch constraining non-detections exist from the CSS, a non-detection from the Mount Lemmon facility (part of CRTS) on the 15th of September 2014 (limiting magnitude of 21.73) constrains the date of explosion to be the 20th of September 2014 ±5 days, or Julian Date (JD) 2456920.5 ±5 days. The transient was also detected much later by Pan-STARRS1 as PS15dsr on the 27th June 2015, at $w_{\rm ps}$ = 21.3 mag. A spectrum was obtained with the *ESO Faint Object Spectrograph and Camera (v.2)* (EFOSC2[35]) mounted on the *New Technology Telescope* (NTT) on September the 29th 2014[36] (see Supplementary Fig. 2), revealing a type II spectral morphology. Matching of the classification spectrum with a library of SN spectral templates using SNID[37] gives good results with SN 2004et at 2 days before maximum light, which translates to 14 days post explosion (+14 d), leading to an explosion epoch of the 15th of September, i.e. the same date as the last non-detection. The reason for the earlier explosion epoch from the spectral matching can be explained by the low progenitor metallicity of SN 2015bs, meaning that spectral line and colour evolution is slower than usually observed in SNe II (because of reduced blanketing by metal lines[38]). Nevertheless, the spectral matching gives an explosion epoch that is overall consistent with that from the non-detection.

We identify narrow Hα emission from a galaxy (indicated in Supplementary Fig. 1) offset

$3.4''$ from SN 2015bs (the characterisation of which is presented below). The observed wavelength of this emission (the only emission line observed for this galaxy) gives a redshift for that object of 0.027. This redshift is consistent with that of the SN Hα emission as seen in the nebular spectrum, and the value inferred from spectral matching above. We adopt this redshift for SN 2015bs, which corresponds to a distance modulus of 35.4 mag (assuming H_0 of 73 km s^{-1} Mpc^{-1}). At this redshift, the angular separation between the peak flux of our identified host and SN 2015bs translates to 2 kpc.

Line of sight extinction from dust contained within the Milky Way is taken from the recalibrated dust maps of [39], assuming a Fitzpatrick extinction law[40]. No sign of narrow sodium absorption within the spectra of SN 2015bs is detected – the presence of which would indicate a higher level of host galaxy extinction – and as shown below in Section 3 and Supplementary Fig. 3, SN 2015bs does not show particularly red colours. Therefore we assume that SN 2015bs is affected by negligible internal host galaxy extinction.

2. Data reduction and calibration

$BVri$ photometry was obtained through the *Carnegie Supernova Project-II* (CSP-II[41]) from around maximum light to just after the end of the plateau, using the Swope telescope (+ e2V CCD) at the Las Campanas Observatory. Images were reduced in a standard manner. Observations of standard star fields were carried out on photometric nights when SN 2015bs was observed allowing the calibration of local standard sequences in BV[42] and ri[43]. Photometry of SN 2015bs was then calibrated against these local sequences, and is published in the natural system of the Swope telescope. Photometry of local sequence stars is presented in Supplementary Table 1 (on the *standard* system), while that of SN 2015bs is listed in Supplementary Table 2 (on the *natural* system). No attempts were made to subtract the underlying host galaxy flux, given that the host is not detected in deep images taken around a year post explosion. The $BVri$ light-curves for SN 2015bs are displayed in Supplementary Fig. 4.

The Pan-STARRS Survey for Transients observed the field of SN 2015bs during the tail phase, some 280 days after discovery during its normal survey mode. The transient was recovered over a period of 77 days with the internal name PS15dsr. The data were taken with the broad w_{ps} band which is a composite of $g_{\mathrm{ps}}r_{\mathrm{ps}}i_{\mathrm{ps}}$, as described in [44]. Difference imaging with respect to a reference frame was carried out, with point-spread-function photometry produced automatically as described in [45] and [46]. The detections from Pan-STARRS difference images are associated and merged into objects in a database of transients[47] and the photometry is reported in Supplementary Table 3 (AB magnitudes in the system described by [48])

Four photospheric-phase optical spectra were obtained for SN 2015bs using the NTT (+ EFOSC2) at La Silla, through the PESSTO collaboration, and using the *Las Cumbres Observatory* (LCO[49]) FLOYDS spectrograph. Spectra were obtained at +9 (the classification spectrum discussed above), +23, +57 and +80 d. The photospheric-phase spectral sequence is presented in Supplementary Fig. 2. EFOSC2 spectra were reduced and calibrated in a standard manner using a custom built pipeline for the PESSTO project[23], while the FLOYDS spectrum was reduced as in [50].

The position and surrounding sky of SN 2015bs were observed using MUSE at +406 and

+421 d. MUSE is a $1' \times 1'$ field of view (FOV) integral field spectrograph, allowing us to simultaneously observe the SN and search for its host galaxy. These data were reduced using the MUSE pipeline[51], with subsequent combination of the two observations. The extracted 1 dimensional spectrum of SN 2015bs is shown in Fig. 2 of the main article. The MUSE data cube was analysed using QFitsView[52].

Throughout our analysis we compare the properties of SN 2015bs with a sample of SNe II from the literature. Given that our conclusions stem from analysis of nebular-epoch optical spectroscopy, our comparison sample was defined as any SN II with a nebular spectrum (with a cut off date of December 2015) within ±50 days of that obtained for SN 2015bs, with respect to the explosion. Seven such SNe were found which are listed in Supplementary Table 4.

3. Nebular line analysis of SN 2015bs with respect to a SN II comparison sample

Nebular spectra of SNe II are dominated by Hα, [O I] 6300,6364 Å, and [Ca II] 7291,7323 Å, and our analysis is restricted to the measurement of these line profiles. We measure FWHM velocities, and in the case of [O I] and [Ca II] their absolute fluxes. Velocities are extracted by fitting Gaussians to each line and measuring their FWHM. In the case of [Ca II], often more than two Gaussians are needed to provide a good fit. This is to be expected, as the [Ca II] lines can be blended with e.g. [Ni II] 7378 Å, [Fe II] 7388 Å, and [Ni II] 7412 Å. In addition, for SN 2015bs and SN 2013ej, more than two components are needed for [O I], and more than one component for Hα (arguing against unusually strong [Ni II] 7378 Å, [Fe II] 7388 Å, and [Ni II] 7412 Å in these SNe II, given that the ‘red-excess’ is not unique to [Ca II]). In the case of SN 2013ej, it has been suggested that the nebular lines are best modelled assuming blue- and red-shifted components of [O I], Hα, and [Ca II][53]. Additional components on the red side of [O I] and Hα were also observed for SN 2014G[54], and were argued to be due to circumstellar interaction. SN 2015bs displays [O I], Hα and [Ca II] emission peaks blue-shifted by around $1000\,\mathrm{kms}^{-1}$. Excess flux is also observed as a red shoulder in emission lines (see Supplementary Figs 8 and 11). Such profiles could suggest significant dust extinction in SN 2015bs. Alternatively, ejecta asymmetries may explain the observed line profiles. Given that we also observe both blue-shifted emission and a red-shoulder excess for [Ca II] 7291,7323 Å suggests that a strong ejecta asymmetry is most likely, as this line predominantly forms outside the metal core where any dust would reside.

If a better fit to the line profiles is attained using additional Gaussian components then these are added, and the [O I], Hα, and [Ca II] velocities are taken from the largest fitted Gaussian. To estimate line fluxes we simply integrate the total emission under the [O I] and [Ca II] line profiles. This is achieved over a constant wavelength range for all SNe, meaning that we include any 'extra' emission observed in the case of [O I], and that from [Ni II] 7378 Å, [Fe II] 7388 Å, and [Ni II] 7412 Å in the case of [Ca II]. This approach is preferred, given the uncertain nature of fitting to multiple unresolved lines, and it also allows for a consistent comparison between all SNe. In this case the values presented here are not immediately comparable to those published elsewhere[31].

Histograms of FWHM velocities of [O I], Hα, and [Ca II] are shown in Supplementary Fig. 7. With respect to the comparison sample, SN 2015bs shows nebular-phase velocities for [O I] and [Ca II] towards the centre of the distributions. However, SN 2015bs clearly displays the highest Hα velocity (Supplementary Figs 8 and 9). Larger nebular-phase velocities are expected in the case of

SNe II with higher helium core masses[4]. As discussed in the main article, we make direct comparison of the nebular-phase Hα velocity measured for SN 2015bs with those from the hydrodynamic models of [4], constraining the progenitor mass of SN 2015bs to be as high as 25 $\mathrm{M}_{\odot}$ (further details below). The 'normal' line velocities for [O I] are to be expected for a larger progenitor mass where a higher percentage of the flux is expected to arise from the core (i.e. a reduced [O I] flux from faster moving outer envelope).

The nebular-line widths are measured directly from the nebular spectrum. However, in order to extract a photospheric-phase velocity – and directly compare observed velocities to model values from [4] – we use two SNe II from our comparison sample to aid us. This is because the spectral lines usually used for estimating the photospheric velocity, such as Fe II 5169 Å are weak in the photospheric-phase spectra of SN 2015bs, making their use unreliable. Therefore, we calibrate the velocity difference between Hβ and Fe II 5169 Å for SN 2004et and SN 2013ej (given their similar Hβ and Hα velocities to SN 2015bs), and apply this difference to the Hβ velocity for SN 2015bs, obtaining a +50 d photospheric velocity of $5359 \pm 392\,\mathrm{kms}^{-1}$. Using this, together with the nebular-epoch HWHM velocity of Hα of $2127 \pm 308\,\mathrm{kms}^{-1}$, thus constrains (through comparison to hydrodynamic models) the initial progenitor mass of SN 2015bs to be between 20 and 25 $\mathrm{M}_{\odot}$.

In the main article the flux of [O I] with respect to the flux of that across the full wavelength range of the MUSE spectrum was presented for SN 2015bs as compared to the same measurement for our comparison sample and SN 1987A. This showed that SN 2015bs indeed displays stronger [O I] with respect to the available energy (^{56}Co decay). Previously, the luminosity of [O I] as a percentage of the total ^{56}Co power at the epoch of observations has been used as a proxy for progenitor mass through model comparisons[13]. Here we also analyse SN 2015bs in this context. To estimate a ^{56}Ni mass for SN 2015bs we proceed with three different methods. Firstly, we extract a synthetic V-band magnitude from the nebular MUSE spectrum obtained at around +400 d, which we estimate to be 24.11±0.66 mag. This magnitude is then converted into a bolometric luminosity, and a ^{56}Ni mass of $0.048^{+0.041}_{-0.022}$ $\mathrm{M}_{\odot}$ is derived assuming full trapping of the radioactive emission by the SN ejecta[55]. Secondly, we integrate the total flux within the MUSE spectrum (4800 to 9300 Å), together with the 'MUSE flux' of a spectrum of SN 1987A close in time to that of SN 2015bs[56]. Converting these fluxes to luminosities we then obtain the ratio of SN 2015bs MUSE luminosity to that of SN 1987A, and using a ^{56}Ni mass of 0.075 for SN 1987A[57], we arrive at a value for SN 2015bs of $0.042^{+0.006}_{-0.007}$ $\mathrm{M}_{\odot}$. Finally, a ^{56}Ni mass is estimated using late-time w_{ps}-band photometry. We first fit a straight line to the w_{ps}-band photometry, confirming a decline rate consistent with that expected by the decay of ^{56}Co. We then extrapolate this (by 50 days) to the epoch at which there is a spectrum available for SN 1987A. A ^{56}Ni mass of $0.057^{+0.003}_{-0.003}$ $\mathrm{M}_{\odot}$ for SN 2015bs is then obtained by scaling the brightness of the SN 2015bs photometry to that of SN 1987A. Taking an average of these three values we obtain a ^{56}Ni mass of 0.049±0.008 $\mathrm{M}_{\odot}$.

Using the derived ^{56}Ni mass for SN 2015bs the luminosity of [O I] is estimated as a percentage of the ^{56}Co power to be 5.3%. This is much higher than any previous SN II (see Fig. 24 of reference [58], where the previous highest value was less than 4%), and when compared to model predictions suggests a ZAMS mass of ≥17-18 $\mathrm{M}_{\odot}$ (estimated from figure 24 of [58]), consistent with the mass estimates from [O I] fluxes as compared to models in the main article using the [O I] flux compared to the total MUSE flux, and comparison to such constraints for SN 1987A.

The overall results from this nebular analysis are shown in Supplementary Fig. 10. Here two ratios are plotted vs. each other. On the x-axis the ratio of the nebular to photospheric-phase Hα velocity is shown. This normalises the outer core velocity to the explosion energy[4]. On the y-axis we show the ratio of the integrated flux of [O I] to that of [Ca II]. SN 2015bs falls on the extreme of the distribution of each axis, confirming its uniqueness. Based on model predictions[4,5], the simplest explanation is that SN 2015bs was the explosion of a massive, 17-25 $\mathrm{M}_{\odot}$ progenitor star, i.e. *the most massive progenitor star* yet inferred for a SN II.

4. Host galaxy identification and characterisation

There is a faint galaxy 12.7″ away from the explosion position of SN 2015bs (see Supplementary Fig. 1), however this galaxy does not have a published redshift and appears as a candidate SDSS galaxy. The initial redshift of 0.021 was taken from the SN spectral matching (see above). This implied an absolute r-band magnitude of –13.6 mag for the galaxy: already one of the dimmest hosts for a SN II. However, in our MUSE observations [O II] 3727 Å and Hβ emission are identified for this galaxy at a redshift of 0.90, inconsistent with our initial redshift estimate and therefore this galaxy was discarded as the possible host. The host of SN 2015bs was identified as a very faint galaxy (see Supplementary Fig. 1) that has narrow Hα emission at a wavelength consistent with SN 2015bs. Only Hα is visible in the spectrum, so we are unable to constrain the metallicity using emission line diagnostics. This provides a compelling argument for the use of SN II as independent metallicity indicators. A synthetic r-band magnitude was extracted from the host galaxy spectrum and estimated to be 23.3±0.2 mag. Correcting this for Milky Way extinction, and the distance modulus, we obtain an absolute r-band magnitude of –12.2, making the host of SN 2015bs the dimmest host for a SN II in the literature. Aware of the caveats of converting this to a metallicity, this implies a chemical abundance of 0.04±0.05 $Z_{\odot}$[19], making SN 2015bs the lowest host metallicity SN II yet studied. The metallicity error is that of the dispersion on the relation between absolute magnitude and metallicity from [19].

Data Availability Statement

The data that support the plots within this paper and other findings of this study are available from the corresponding author upon reasonable request. In addition, the PESSTO spectra are available through the PESSTO Spectroscopic Data release 3 (SSDR3), for more information see the PESSTO website (`www.pessto.org`), all spectra will also be made available on WISeREP: `www.weizmann.ac.il/astrophysics/wiserep/`, and photometric measurements are listed in the SI.

References

34. Bacon, R. *et al.* MUSE Commissioning. *Msngr*. **157**, 13-16 (2014)

35. Buzzoni, B. *et al.* The ESO Faint Object Spectrograph and Camera (EFOSC). *Msngr*. **38**, 9-13 (1984).

36. Walton, N., et al. PESSTO spectroscopic classification of optical transients. *ATEL*. **6516**, 1

(2014)

37. Blondin, S. & Tonry, J. L. Determining the Type, Redshift, and Age of a Supernova Spectrum. *Astrophys. J.* **666**, 1024-1047 (2007)

38. Dessart, L. & Hillier, D. J. Non-LTE time-dependent spectroscopic modelling of Type II-plateau supernovae from the photospheric to the nebular phase: case study for 15 and 25 M $\mathrm{M}_{\odot}$ progenitor stars. *Mon. Not. R. Astron. Soc.* **410**, 1739-1760 (2011)

39. Schlafly, E. F. & Finkbeiner, D. P. Measuring Reddening with Sloan Digital Sky Survey Stellar Spectra and Recalibrating SFD. *Astrophys. J.* **737**, 103-126 (2011)

40. Fitzpatrick, E. L. Correcting for the Effects of Interstellar Extinction. *Pub. Astro. Soc. Aust.* **111**, 63-75 (1999)

41. Hamuy, M. *et al.* The Carnegie Supernova Project: The Low-Redshift Survey. *Pub. Astro. Soc. Aust.* **118**, 2-20 (2006)

42. Landolt, A. U. UBVRI photometric standard stars in the magnitude range 11.5-16.0 around the celestial equator. *Astron. J.* **104**, 340-371 (1992)

43. Smith, J. *et al.* The u'g'r'i'z' Standard-Star System. *Astron. J.* **123**, 2121-2144 (2002)

44. Chambers, K. C. *et al.* The Pan-STARRS1 Surveys. *arXiv*. 1612.05560 (2016)

45. Waters, C. Z. *et al.* Pan-STARRS Pixel Processing: Detrending, Warping, Stacking. *arXiv*. 1612.05245 (2016)

46. Magnier, E. A. *et al.* Pan-STARRS Photometric and Astrometric Calibration. *arXiv*. 1612.05242 (2016)

47. Smartt, S. J. *et al.* Pan-STARRS and PESSTO search for an optical counterpart to the LIGO gravitational-wave source GW150914. *Mon. Not. R. Astron. Soc.* **462**, 4094-4116 (2016)

48. Tonry, J. L. *et al.* The Pan-STARRS1 Photometric System *Astrophys. J.* **750**, 99-103 (2012)

49. Brown, T. M. *et al.* Las Cumbres Observatory Global Telescope Network *Pub. Astro. Soc. Aust.* **125**, 1031 (2013)

50. Valenti, S. *et al.* The first month of evolution of the slow-rising Type IIP SN 2013ej in M74 *Mon. Not. R. Astron. Soc.* **438**, L101-L105 (2014)

51. Weilbacher, P. M. *et al.* The MUSE Data Reduction Pipeline: Status after Preliminary Acceptance Europe. *ASPC*. **485**, 451 (2014)

52. Ott, T. QFitsView: FITS file viewer. *ASCL*. 10019 (2012)

53. Yuan, F. *et al.* 450 Days of Type II SN 2013ej in Optical and Near-Infrared. *Mon. Not. R. Astron. Soc.* **461**, 2003-2018 (2016)

54. Terreran, G. *et al.* The multi-faceted Type II-L supernova 2014G from pre-maximum to nebular phase. *Mon. Not. R. Astron. Soc.* **462**, 137-157 (2016)

55. Hamuy, M. Observed and Physical Properties of Core-Collapse Supernovae. *Astrophys. J.* **582**, 905-914 (2003)

56. Phillips, M. M. *et al.* An optical spectrophotometric atlas of supernova 1987A in the LMC. II - CCD observations from day 198 to 805. *Astron. J.* **99**, 1133-1145 (1990)

57. Arnett, D. Supernovae and Nucleosynthesis. *Princeton University Press*. (1996)

58. Valenti, S. *et al.* The diversity of Type II supernova versus the similarity in their progenitors. *Mon. Not. R. Astron. Soc.* **459**, 3939-3962 (2016)

Figure 2 Absolute V-band light-curves of SN 2015bs together with a comparison sample from the literature. The light curve of SN 2015bs is shown in light blue. Errors on the photometry of SN 2015bs are the propagated errors from the photometric calibration (those for the comparison sample are taken from the literature). While SN 2015bs falls on the bright side of the distribution, overall it displays a normal light-curve morphology for a SN II. The decline rate during the 'plateau' phase appears typical of SNe II, as does the length of the optically thick phase duration.

Figure 3 Comparison of the 57 d spectrum of SN 2015bs with 0.1 $\mathrm{Z}_\odot$ and 0.4 $\mathrm{Z}_\odot$ models at +50 d[3]. We also present an example SN II from our comparison sample (SN 2012aw) which shows much more prominent metal lines, more consistent with the 2 $\mathrm{Z}_\odot$ model. It is clear that the 0.1 $\mathrm{Z}_\odot$ model best matches the spectrum of SN 2015bs (observe the regions bluer than 5000 Å, and specifically the strength of the Fe II 5018 Å line, which is bracketed by dashed lines), providing strong evidence for the low-metallicity nature of SN 2015bs.

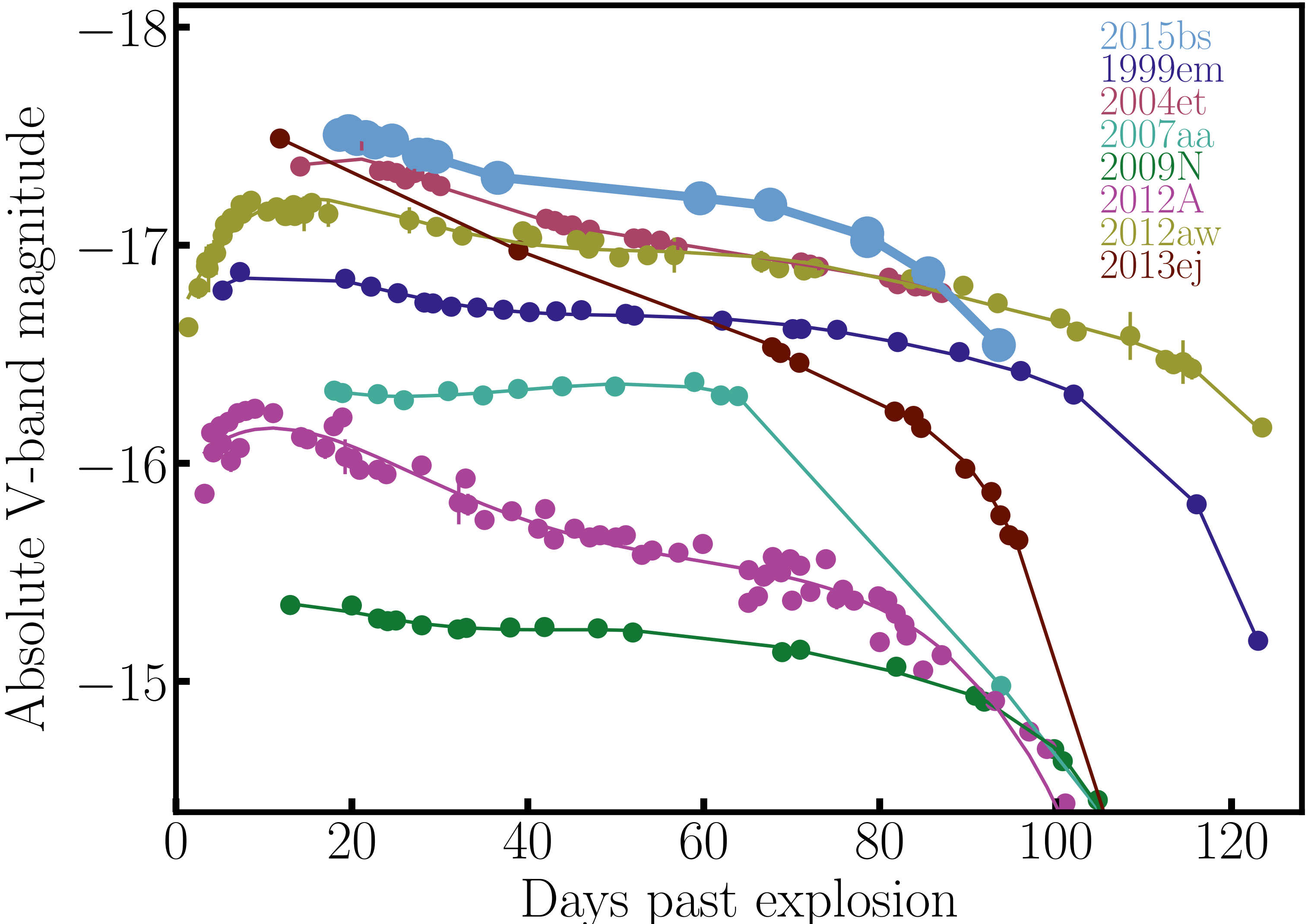
2015bs
1999em
2004et
2007aa
2009N
2012A
2012aw
2013ej
Absolute V-band magnitude
−18
−17
−16
−15
Days past explosion
0
20
40
60
80
100
120

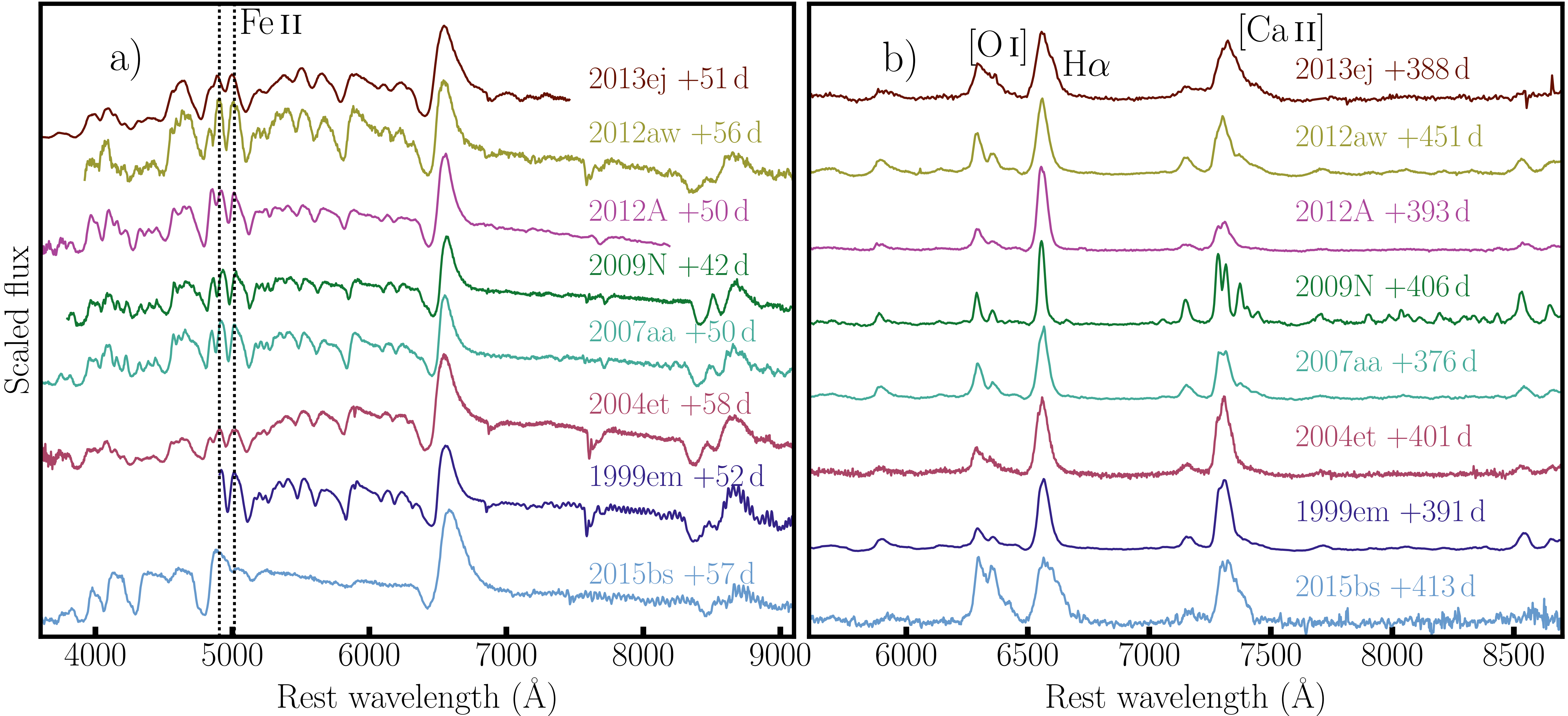
a)
Fe II
2013ej +51 d
2012aw +56 d
2012A +50 d
2009N +42 d
2007aa +50 d
2004et +58 d
1999em +52 d
2015bs +57 d
Scaled flux
4000
5000
6000
7000
8000
9000
Rest wavelength (Å)
b)
[O I]
Hα
[Ca II]
2013ej +388 d
2012aw +451 d
2012A +393 d
2009N +406 d
2007aa +376 d
2004et +401 d
1999em +391 d
2015bs +413 d
6000
6500
7000
7500
8000
8500
Rest wavelength (Å)

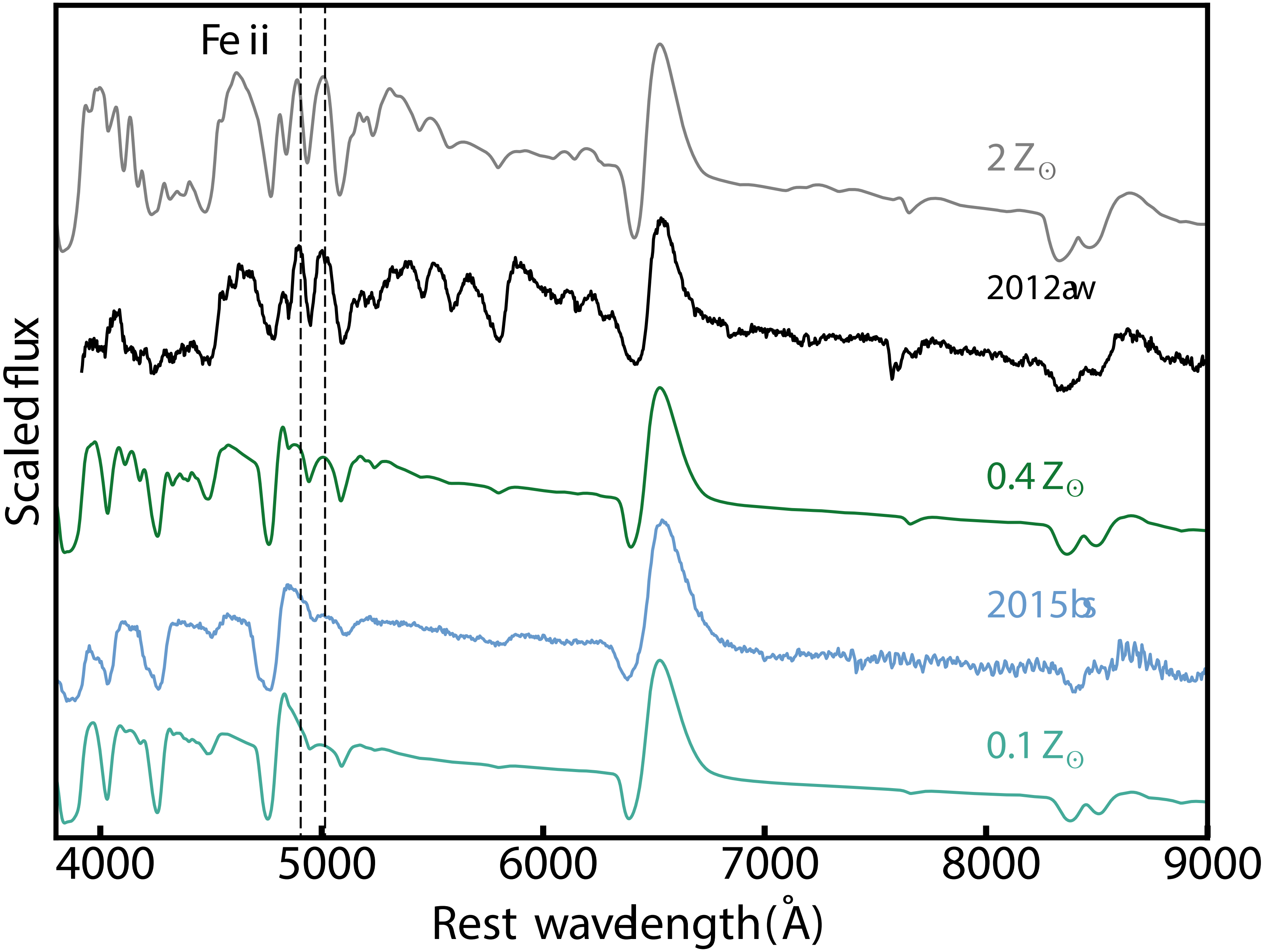

Fe ii
2 Z⊙
2012aw
0.4 Z⊙
2015bs
0.1 Z⊙
Scaled flux
4000
5000
6000
7000
8000
9000
Rest wavelength (Å)